Plasma Chem Plasma Process (2012) 32:801–816
DOI 10.1007/s11090-012-9378-8

ORIGINAL PAPER

On the Use of Atmospheric Pressure Plasma for the Bio-Decontamination of Polymers and Its Impact on Their Chemical and Morphological Surface Properties

K. Fricke · H. Tresp · R. Bussiahn · K. Schröder · Th. von Woedtke · K.-D. Weltmann

Received: 21 April 2011 / Accepted: 12 April 2012 / Published online: 11 May 2012

Abstract Low temperature atmospheric pressure plasma processes can be applied to inactivate micro-organisms on products and devices made from synthetic and natural polymers. This study shows that even a short-time exposure to Ar or Ar/O_2 plasma of an atmospheric pressure plasma jet leads to an inactivation of *Bacillus atrophaeus* spores with a maximum reduction of 4 orders of magnitude. However, changes in the surface properties of the plasma exposed material have to be considered, too. Therefore, polyethylene and polystyrene are used as exemplary substrate materials to investigate the effect of plasma treatment in more detail. The influence of process parameters, such as type of operating gas or jet-nozzle to substrate distance, is examined. The results show that short-time plasma treatment with Ar and Ar/O_2 affects the surface wettability due to the introduction of polar groups as proofed by X-ray photoelectron spectroscopy. Furthermore, atomic force microscopy images reveal changes in the surface topography. Thus, nano-structures of different heights are observed on the polymeric surface depending on the treatment time and type of process gas.

Keywords Atmospheric pressure plasma jet · Polymers · Decontamination · Modification · XPS · AFM

Introduction

Heat sensitive materials like polymers used for biomedical applications (e.g. medical implants) often undergo various pre-treatments to obtain desired physico-chemical surface characteristics to ensure reliable functionality in the biological environment [1–3]. For further processing, an activation of the substrate surface is required as well as a sterile handling. In this case, gas-discharge plasma-based processes are the method of choice, combining the change of chemical and physical properties of only the outermost layer of

K. Fricke (✉) · H. Tresp · R. Bussiahn · K. Schröder · Th. von Woedtke · K.-D. Weltmann
INP Greifswald e.V., Leibniz Institute for Plasma Science and Technology, Felix-Hausdorff-Str. 2, 17489 Greifswald, Germany
e-mail: k.fricke@inp-greifswald.de

the polymer surface without affecting the bulk properties and the ability to bio-decontaminate the surface at the same time. Furthermore, plasmas have a great potential to modify and/or bio-decontaminate small and complex-shaped products regarding the inherent advantages of gas phase processes [4]. A physical plasma is created from a gas that is dissociated and ionized. It is a quasineutral particle system composed of positively and negatively charged ions, radicals, electrons, and neutral particles (atoms, molecules) [5]. Owing to the moderate neutral gas temperatures (at or near ambient temperature), non-thermal plasmas are more suitable for the sterilization or modification of thermolabile polymeric surfaces. In particular, atmospheric plasma processes are of growing interest, since they do not require expensive vacuum systems which reduces the process cost significantly. Therefore, the number of newly developed plasma sources designed for surface functionalization and biological decontamination has grown considerably within the last years [6–9]. Non-thermal plasmas provide several types of active species including charged particles, radicals, excited metastables, electric fields, and (V)UV radiation, which are considered to be effective sterilizing agents [10, 11]. However, these plasma-generated species are not only capable to inactivate micro-organisms, they may also initiate reactions with polymer surfaces [12]. Hence, it is necessary to investigate the plasma induced surface modification during antimicrobial treatment in detail, as surfaces modified in this manner exhibit changes in wettability, elemental composition, and texture (roughness) leading to alteration of the functionalities [13, 14]. It is thus possible to obtain required surface bio-decontamination and at the same time improved surface properties to accomplish biocompatibility, which is especially for biomedical materials of importance. For instance, chemical functionalities such like hydroxyls, carboxyl groups, ketones, and aldehydes can be created on the surface during plasma exposure causing an increase of surface energy and subsequently an improved wettability, which in turn enables a better adhesion and proliferation of cells [15, 16]. Nevertheless, changes in the surface morphology and topology induced by the plasma treatment facilitate an appropriate biological response, too [17, 18].

Since gas plasma bio-decontamination/sterilization of heat sensitive materials is considered to be a prospective alternative to commercial available methods, the present work is focused on the inactivation of *Bacillus atrophaeus* spores using argon and argon oxygen plasma. Furthermore, the inactivation efficiency was compared dependent on the process gas, treatment time, and operating distance. In parallel with the antimicrobial studies, the changes in the physico-chemical surface properties of polyethylene (PE) and polystyrene (PS) were also examined. Therefore, water contact angle measurements, atomic force microscopy (AFM), and X-ray photoelectron spectroscopy (XPS) were applied. Additional optical emission spectroscopy (OES) studies were performed to obtain more information on the species present in the plasma.

Experimental Set Up

Miniaturized Atmospheric Pressure Plasma Jet

The principal set up of the high-frequency (HF) driven (1.7 MHz) miniaturized atmospheric pressure plasma jet (kINPen, INP Greifswald, Germany) is schematically shown in Fig. 1. The device consists of a grounded ring electrode and a centered rod electrode inside a quartz capillary (with an inner diameter of 1.6 mm and an outer diameter of 4 mm) which is coupled to the power source via a matching network. Throughout the experiments

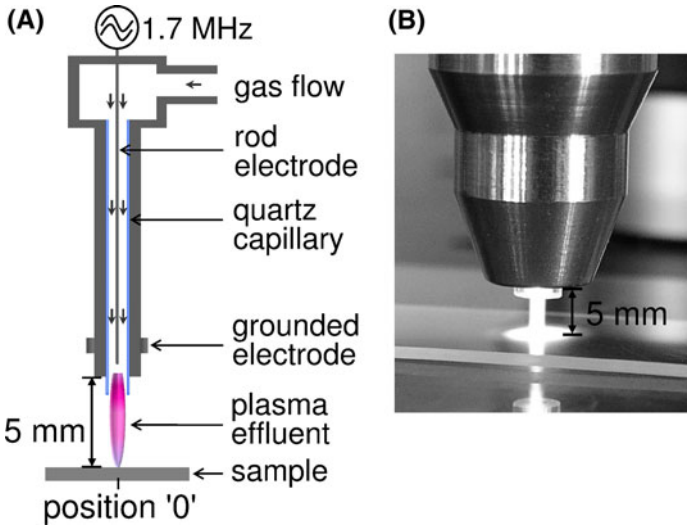

Fig. 1 **a** Experimental set-up and scheme of the plasma jet (kINPen). **b** Photograph of the Ar plasma jet impinging on a PS substrate at a jet-nozzle to substrate distance of 5 mm

the overall electric power applied to the device was held constant at 65 W (as measured at the generator output). The plasma source was operated with argon at a flow rate of 5 standard liter per minute (slm) and small admixtures of molecular oxygen of up to 0.05 slm (1 %O_2). Under these conditions, the length of the Ar plasma jet expanding into the surrounding air was observed to be 12 mm and with 1 % oxygen admixture 5–6 mm from the nozzle outlet. It has to be noted, that for this reason at a jet-nozzle to substrate distance (also called axial distance) of 5 mm the Ar plasma jet spreads on the polymeric substrate. Thus, the impinging jet affects a surface area in the range of 5–7 mm. Further details on this type of jet are described elsewhere [19, 20]. The plasma treatments were performed only at one position (localized treatment) of the polymer surfaces which is labeled as position '0'.

Polymeric Materials

The experiments were carried out with polyethylene (PE, 200 μm thick, 0.94 g/cm^3, Goodfellow, Germany) and polystyrene (PS, 125 μm thick, 1.02 g/cm^3, Greiner, Germany) as substrate materials. Polyethylene and polystyrene are hydrocarbon polymers with a simple chemical structure containing no chemical functional groups which facilitates clear information on the impact of plasma on the chemical surface composition. Furthermore, these polymers were selected because of their particular relevance in biomedical applications.

Microbiological Tests

For the microbiological tests endospores of *B. atrophaeus* spores were used due to their standardized usage for sterilization processes [22]. Endospores are inactive or dormant forms of bacteria. Compared to vegetative forms (actively growing) spores are most

resistant to chemical and environmental factors such as chemical agents, heat, radiation, and changes in pH.

Inactivation kinetics of micro-organisms by plasma have been realized using polyethylene and polystyrene strips (3 × 0.9 cm) contaminated punctually with 25 µl of a suspension of *B. atrophaeus* spores (drop diameter: 3–4 mm) and dried under aseptic conditions. The plasma-treated strips as well as the non-treated strips (control) were transferred into tubes containing 10 ml sterile tryptic soy broth and agitated for 15 min on a Bühler shaker to remove vital and destroyed spores. Afterwards, the culture vessels were put into a water bath of 80 °C for 10 min to destroy vegetative germs. The spore concentration was quantified via dilution series by the surface-spread plate count method using agar plates (Caso, Merck) and is given as colony forming units per object (CFU/object). The plates were incubated for at least 20 h at 36 °C. For each experiment three samples were treated at a time under the same conditions for statistics.

Surface Analysis

Contact angle measurements on the polymer surfaces were performed under ambient air at room temperature by the sessile drop method using a Digidrop contact angle analyzer (GBX Instrumentation Scientifique, France) and a drop of distilled water with a defined volume (0.5 µl). The contact angle was measured through the zone of the locally plasma-treated polymer (line scan) with a step width of 3 mm. The contact angle of the resting drop was determined utilizing the software Windrop. The chemical composition of the surfaces was measured ex-situ with X-ray photoelectron spectroscopy (XPS) (Axis Ultra, Kratos, Manchester, UK) utilizing monochromatic aluminum K_α irradiation at 1,486.6 eV. Charge neutralization was implemented by low energy electrons, injected in the magnetic field of the lens from a filament located directly atop the sample. The spot size was ca. 250 µm in diameter. Wide scans and element spectra were recorded at a pass energy of 80 eV for the estimation of the chemical element composition and at a pass energy of 10 eV for the highly resolved measurements of the C 1s peak, respectively. Data acquisition and processing were carried out using the software CasaXPS, version 2.14.dev29 (Casa Software Ltd., Teignmouth, UK). A line scan through the centre of the plasma-treated zone of the polymeric substrates was recorded with a step size of 0.5 mm. All values are given in XPS atomic percent. Curve-fitting of the highly resolved C 1s region was performed to characterize the chemical structure of the polymeric surface using Gaussian–Lorentzian distribution and a linear baseline. The full width at half maximum of the C 1s components was 1.2 eV for high energy resolution measurements. Atomic force microscopy (AFM) provides the determination of the surface topography before and after plasma treatment. The AFM analysis was performed with a scanning probe microscope diCP-II (Veeco Instruments, Santa Barbara, USA) in the non contact mode, especially tapping mode. An area of 10 × 10 µm was scanned using a pyramidal silicon tip doped with n-type phosphorus with a resonance frequency of 273–389 kHz and a force constant of 20–80 N/m (Veeco, RTESPA-CP). Five areas were recorded for each sample and analyzed by means of the software SPMLab Ver. 6.0.2 (Veeco).

Optical Emission Spectroscopy

For the optical emission spectroscopy (OES) a dual channel fiber optical spectrometer (Avantes AvaSpec 2048-2-USB2) was used. The first channel operated in the range of UV/VIS (200–450 nm) with a grating (600 lines/mm, Blaze 250 nm) and a 25 µm slit. The

resolution of this channel was 0.6 nm. Channel two operated in the range of 450–950 nm (25 μm slit, 600 lines/mm, Blaze 500 nm) with a resolution of 0.7 nm. The channels were linked to a y-cable, which had a 0.6 mm core and was coupled with a second fiber (diameter 1 mm). The spectra were normalized to the exposure time and relatively calibrated. The OES spectra were recorded side-on, i.e. the fiber was located lateral to the jet plasma, from the jet-nozzle up to the end of the plasma jet and analyzed using the software Spectrum Analyzer [21].

Results and Discussion

Antimicrobial Treatment

Bio-decontamination (inactivation or removal of micro-organisms on surfaces) or sterilization (complete absence of all viable micro-organisms) of surfaces has become one of the most important topics in gas-discharge based surface treatment [22, 23]. Especially for sensitive surfaces and goods which cannot be treated with conventional sterilization methods, such like heat sterilization, alternative and non-invasive approaches have to be evaluated. Gas-discharges are well-suited for treating sensitive substrate surfaces, e.g. of thermolabile substrates like polymers. Therefore, different plasma sources were developed with the purpose of bio-decontamination and additionally, the process of plasma-induced inactivation of bacteria cells is well discussed [4, 22]. Hence, only a brief outline is given here about the bio-decontamination potential of the applied plasma jet by using *B. atrophaeus* spores as test organism.

Plasma inactivation kinetics of *B. atrophaeus* spores for different operating gases and axial distances are depicted in Fig. 2. In particular, in Fig. 2a the spore viability (counts of colony forming units (CFU)) after plasma exposure applying different gas mixtures as a function of treatment time is plotted. As process gases pure argon and argon with admixtures of 0.2 and 1 % oxygen were used. The dashed line in this figure represents the detection limit of 100 CFU/object caused by the used method. If no spores were found on the samples the value of the detection limit was used. As shown in Fig. 2a the number of CFU was reduced with increasing treatment time. In terms of the process gas an enhanced plasma inactivation efficacy of *B. atrophaeus* spores was observed when oxygen was added. Particularly, for treatment times above 30 s considerable differences concerning the microbicidal efficiency of Ar and Ar/O_2 plasma were observed. Thus, by using oxygen admixtures an increase of the lethal effect by one log reduction was observed. Furthermore, dependent on the amount of added oxygen an improved lethal effect was achieved with the highest feasible oxygen admixture of 1 %. Hence, a maximum reduction of four orders of magnitude of the initial concentration was obtained after a treatment time of 180 s using Ar/O_2 (1 % O_2) plasma (see Fig. 2a). The mechanism of the microbicidal action of plasma results from different plasma-generated species. In detail, the lethal effect of argon plasma is mainly based on (V)UV radiation validated by optical emission spectroscopy, which for example exhibits lines in the UV-B, UV-A, and VUV region [19, 20, 24]. Lange and von Woedtke investigated the influence of (V)UV radiation of the atmospheric pressure plasma jet on the inactivation of *B. atrophaeus* spores and found that this radiation is crucial for the lethal effect when pure argon is used [22]. However, when oxygen is admixed to the argon plasma reactive species like O and O_3 are generated, which are known for their antimicrobial effect and consequently increase the bacteria inactivation significantly [25, 26]. Figure 3 exemplarily shows optical emission spectra of Ar plasma and Ar/O_2

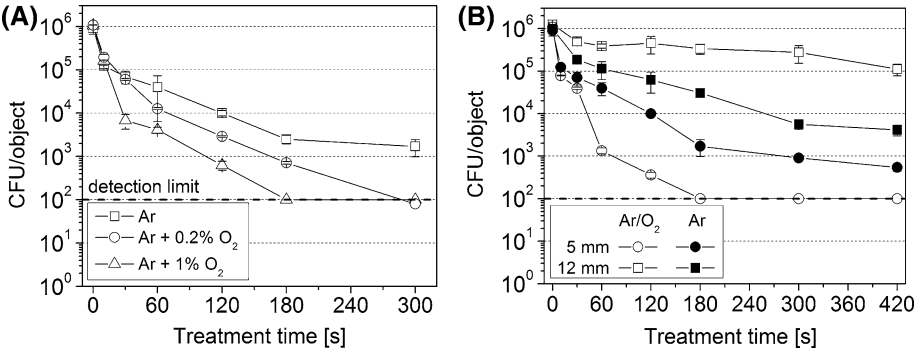

Fig. 2 Inactivation curves of *B. atrophaeus* spores (number of viable micro-organisms in CFU/object): **a** after Ar (*open square*), Ar + 0.2 % O_2 (*open circle*), and Ar + 1 % O_2 (*open triangle*) plasma treatment on punctually contaminated PS strips. The jet-nozzle to substrate distance was 5 mm. **b** exposed to Ar (*filled symbols*) and Ar + 1 % O_2 (*open symbols*) plasma at jet-nozzle to substrate distances of 5 mm (*circles*) and 12 mm (*squares*) on punctually contaminated PE strips. The *dashed horizontal line* indicates the detection limit. (mean ± SD, n = 3 each)

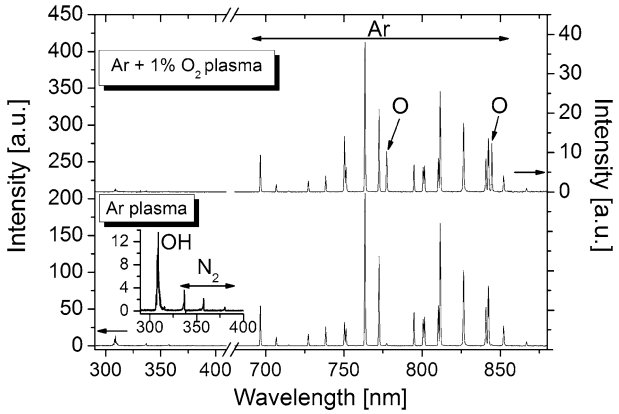

Fig. 3 Typical optical emission spectra of Ar (*lower graph*) and Ar/O_2 (1 % O_2) (*upper graph*) plasma recorded side-on close to the jet-nozzle (axial position of 3 mm). The inset in the lower graph shows the magnification for wavelengths between 290 and 400 nm in the Ar gas discharge

(1 % O_2) plasma recorded at a distance of 3 mm from the nozzle outlet. The emission spectrum of the argon discharge in the visible range was dominated by atomic lines of argon whereas in the region between 300 and 400 nm emission of OH at 308 nm and of the second positive system of molecular nitrogen N_2 at 337 nm were observed. The OES spectrum of argon-oxygen plasma showed high intensity lines of atomic oxygen at 777 nm and at 844.6 nm which are caused by the dissociative excitation and the direct excitation processes. The intensities of OH and N_2 lines were comparatively weak. Consequently, the admixture of oxygen results in quenching of N_2 and OH lines [27]. The spectrum of Ar plasma showed also a slight emission of oxygen but the emission intensity of atomic O (I_O) at 844.6 nm compared to the emission intensity of Ar (I_{Ar}) at 750.4 nm for the two different process gases showed distinctive differences. The I_O/I_{Ar} ratio of the Ar discharge was 0.07 whereas an I_O/I_{Ar} ratio of 0.87 was determined for the Ar/O_2 discharge. Thus, the

emission of excited atomic oxygen was ten fold higher when 1 % oxygen was added. According to this result and due to the fact that the excitation and generation of N_2 and OH is suppressed when oxygen is added it can be assumed, that the enhanced lethal effect of Ar/O_2 plasma might derive from the presence of plasma-generated reactive oxygen species. Dobrynin et al. [28] also studied the influence of the gas composition on the inactivation of bacteria and pointed out that oxygen is required for fast and effective biodecontamination. However, not only the process gas has an influence on the inactivation efficacy but also the operating distance which is displayed in Fig. 2b for Ar and Ar/O_2 (1 % O_2) plasma. For this purpose polymeric samples were positioned at a distance of 5 mm up to 12 mm from the jet-nozzle. Figure 2b shows that the inactivation efficiency was decreased when the jet-nozzle to substrate distance was increased, most of all when oxygen was admixed. This experimental observation can be attributed to the longer pathway of reactive species, the short lifetimes of oxygen atoms (in the range of ms [29]), and the reaction with ambient air, so that the number of reactive species reaching the surface and potentially inactivating the micro-organisms is reduced. Additionally, it can be assumed that the area of the polymer strip covered by the plasma is distinctly lessens with increasing operating distance, especially when oxygen is added due to the reduced length of the jet's effluent. Therefore, at a jet-nozzle to substrate distance of 12 mm a reduction by one order of magnitude was observed after 420 s of Ar/O_2 plasma exposure while at a jet-nozzle to substrate distance of 5 mm only 30 s were needed to obtain the same result. Based on these observations further OES measurements were performed to investigate the axial distribution of excited species generated by Ar (Fig. 4a) and Ar/O_2 plasma (Fig. 4b, note that the axial distance is reduced to 7 mm because of the shortened plasma jet when oxygen is admixed). The results obtained from the optical emission spectroscopy revealed that the intensity of the excited species of Ar, OH, and O was highest close to the nozzle outlet and decreased towards the end of the plasma jet. This observation correlates very well with the decreased lethal effect of plasma at higher axial distances. In contrast, the intensity of the second positive system of N_2 increased with the distance to the jet-nozzle showing a maximum at a distance of 9 mm in the Ar discharge (Fig. 4a) which was also observed by Bornholdt et al. [30]. This result indicates the interaction of the ambient air with the jet effluent leading to the excitation of nitrogen. Bornholdt et al. assumed that

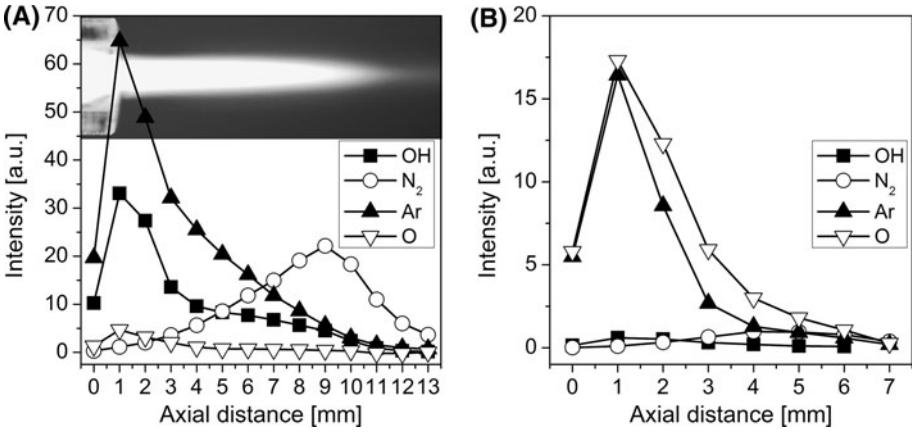

Fig. 4 Intensity of excited species (Ar: 750.4 nm, O: 844.6 nm; OH: 308 nm N_2: 337 nm) in **a** Ar plasma and **b** Ar/O_2 (1 % O_2) plasma depending on the axial distance

especially excited (metastable) argon atoms and UV radiation are involved in the generation of N_2.

It should be noted that the influence of heat produced by the plasma jet on the inactivation of *B. atrophaeus* spores can be excluded here. Spores of *B. atrophaeus* are coated with a complex multilayer (spore coat) composed of several proteins which increase the resistance to the antimicrobial effect of chemical and physical components [31]. Furthermore, Brandenburg et al. showed that a hot air stream with temperatures between 80 and 90 °C did not reduce the initial spore concentration due to the high temperature resistance of *B. atrophaeus* spores [32]. Additionally, the atmospheric pressure plasma jet offers the possibility to operate in the burst mode (constant period of HF voltage supply—plasma on—is followed by a break period—plasma off) which can reduce the temperature load of the target without losing the antimicrobial efficacy. For detailed information the interested reader is referred to Weltmann et al. [19].

Summarizing, the admixture of oxygen and a short distance between the jet-nozzle and the substrate are needed with this plasma jet for a sufficient bio-decontamination. Similar results were published by Lim et al. [26]. He achieved the best inactivation adding oxygen to the argon plasma jet operating at short exposure distances with a reduction factor of 6 after 30 s Ar/O_2 plasma. Whereas Brandenburg et al. [32] obtained a reduction of 4 orders of magnitude after 420 s using pure argon plasma at atmospheric pressure.

Surface Modification

Besides the antimicrobial effects the plasma-induced physico-chemical properties of the polymeric surfaces were studied as well. In particular the influence of the plasma treatment on the polymer modification and etching was of interest here. The physico-chemical properties are of importance since they determine adhesion, repulsion, and wettability of the newly generated interface.

The radial profile of the wettability after plasma treatment, in detail the evolution of the water contact angle on polyethylene and polystyrene along a line crossing the substrate centre with a step size of 3 mm, is shown in Fig. 5. Note, that '0' represents the position of

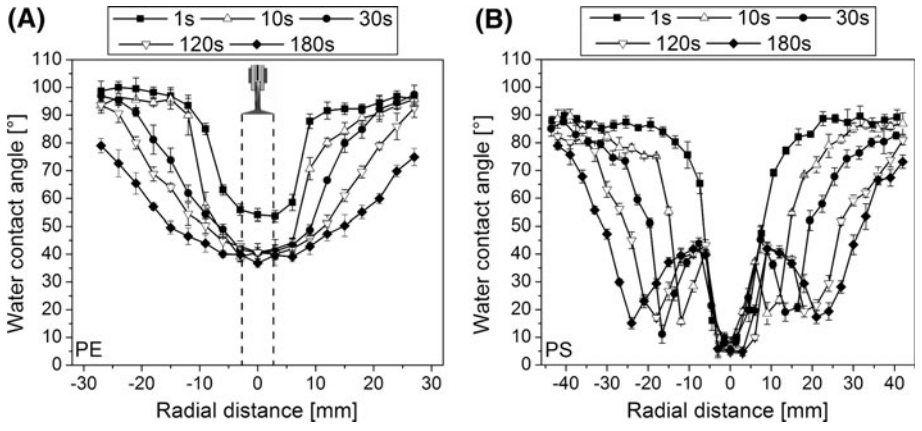

Fig. 5 Radial profile of the water contact angle on **a** PE and on **b** PS after Ar plasma treatment depending on treatment time (mean ± SD, n = 3 each). The jet-nozzle to substrate distance was 5 mm. Also shown in Fig. 5a is a schematic plot of the dimension of the active plasma zone under the given treatment conditions

the localized jet treatment. These measurements were performed to obtain initial information on the altered surface properties immediately after plasma treatment. Since the water contact angle measurements were restricted to the sessile drop method the data presented here indicate changes in the wettability of the polymer only. Furthermore, the variation of the contact angle across the substrate exhibited the extensive impact of the plasma on the surface properties. Anyway, it was possible to receive general information on the influence of the plasma treatment on the surface wettability. E.g., the initial contact angle of 100° was reduced to a minimum contact angle of 40° after 30 s plasma treatment for PE (Fig. 5a) and from 90° to 5° after 1s plasma treatment for PS (Fig. 5b), respectively. Furthermore a time-dependent broadening of the profile was observed due to a radial flowing afterglow of the plasma jet [33, 34]. Thus, a surface modification beyond the impinging jet was caused after a few seconds, already. Additionally, the contact angle measurements showed that the maximum contact angle reduction was achieved within a few seconds of plasma exposure and that it reached a constant value shortly after. The radial distribution of the contact angle showed different profiles for PE and PS. For PE a single minimum at the centre of the substrate (at position '0') was observed with a broadened profile with increasing treatment time (Fig. 5a). PS showed a similar tendency for short treatment times only. After longer treatment time (>10 s) another effect was observed. In addition to the center dip a ring-shaped minimum appeared, indicated as two side-minima in the radial profile of PS (Fig. 5b). The width of the centre dip was nearly constant for all treatment times whereas a broadening of the total modified area with treatment time was observed too. The influence of the jet-nozzle to substrate distance on the wettability of PE and PS showed minimal changes. The inset in Fig. 6 displays the evolution of the water contact angle of PE determined at different axial distances after 60 s Ar plasma treatment. Even at higher axial distances (above 15 mm) a hydrophilicity of the polymer surface was observed. In comparison to small distances, where the contact angles varied between 33 and 44°, the contact angles were here between 48 and 52°. Regarding the effect of the process gas on the surface wettability, different oxygen admixtures (up to 1 %) did not result in remarkable differences compared to pure Ar plasma [33]. For a more detailed understanding of the plasma-assisted surface functionalization the chemical

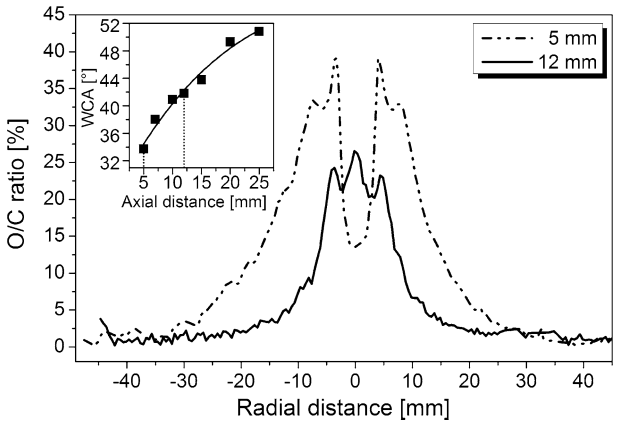

Fig. 6 Radial profile of the O/C ratio of PE exposed to Ar plasma for 60 s at jet-nozzle to substrate distances of 5 (*straight line with dash*) and 12 mm (*straight line*). *Inset*: Dependence of the water contact angle (WCA) on the jet-nozzle to substrate distance (Treatment conditions: Ar plasma, 60 s)

composition of the polymer surface and the carbon binding state of PE and PS before and after plasma treatment was investigated by XPS. Table 1 contains the elemental composition of PE and PS dependent on the process gas and treatment time determined at position '0' of the polymeric surface. In general, non-treated PE and PS are only composed of hydrocarbons. Nevertheless, XPS analysis revealed residues of oxygen (O/C <0.5 %) on non-treated PE and PS associated with contaminations of the surrounding air. However, the results presented in Table 1 indicate a significant oxidation of plasma-treated surfaces which is shown by the remarkable increase in the oxygen-content after plasma exposure which is caused by reactions of plasma-generated active surface sites with oxygen-containing radicals from the plasma or by post-plasma processes with ambient air. Furthermore, with prolonged treatment time the O/C ratio of the PE and PS surface was increased. In terms of different process gases a further increase of the O/C ratio after Ar/O_2 (1 % O_2) plasma was observed. Besides oxygen also nitrogen and silicon were detected. Nitrogen was observed on PE and PS after Ar plasma treatment only but not after Ar/O_2 exposure ascribe to the suppression of the N_2 production when oxygen is admixed. The silicon originated probably from the quartz capillary of the jet or from contamination of the polymer caused by the manufacturing process because silicon was not detected for every measurement after plasma treatment. Since the plasma-modified surfaces showed remarkable changes in the carbon and oxygen content, only the O/C ratio will be discussed in more detail. Radial profiles of the O/C ratio for PE and PS after 60 s Ar plasma exposure are exemplarily shown in Figs. 6 and 7. In particular, Fig. 6 shows the radial profile of the O/C ratio on plasma-treated PE dependent on the jet-nozzle to substrate distance. It was found that at an axial distance of 5 mm, the evolution of the O/C ratio on the PE surface can be observed across 50 mm, while the modified area at an axial distance of 12 mm was reduced to a width of 20 mm. Furthermore, the maximum O/C ratio decreased with axial distance which consequently resulted in a decreased hydrophilicity which is shown in the inset of Fig. 6. Besides the decreasing wettability with decreasing O/C ratio, further differences concerning the variation of the O/C ratio can be observed. Whereas at a jet-nozzle to substrate distance of 5 mm the incorporation of oxygen starts far away of the impinging jet, the oxygen content determined at a distance of 12 mm was highest in the centre of the plasma treatment. However, a comparison of the radial profile of the O/C ratio obtained for PE (Fig. 6, dashed line) and PS (Fig. 7, solid line) after 60 s Ar plasma treatment showed

Table 1 Surface chemical composition (in atom %) of PE and PS dependent on the treatment time and the gas mixture composition (5 slm Ar and 5 slm Ar + 0.05 slm O_2)

	PE			PS		
	C	O	O/C	C	O	O/C
Non-treated	99.7	0.3	0.3	99.5	0.5	0.5[b]
30 s Ar	84.9	15.1	17.8	88.9	10.1	11.4
30 s Ar/O_2	85.1	14.9	17.5	85.6	13.3	15.5[b]
60 s Ar	86.1	13.2	15.5[a]	86.6	13.4	15.5
60 s Ar/O_2	85.9	14.1	16.4	86.2	13.8	16.0
180 s Ar	86.0	13.4	15.6[b]	84.5	14.0	16.6[a,b]
180 s Ar/O_2	84.1	15.8	18.8[b]	83.5	15.7	18.8[b]

[a] Traces of N <0.9 %

[b] Traces of Si <0.8 %

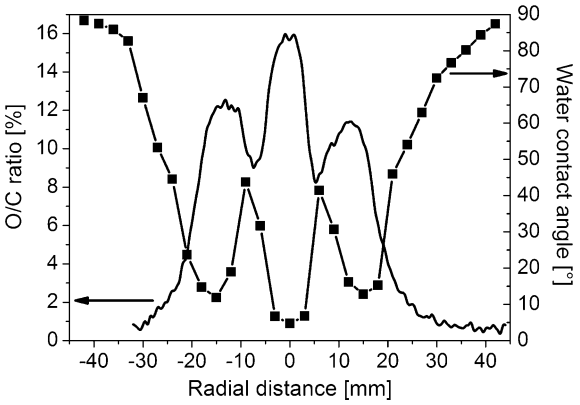

Fig. 7 Radial profile of the O/C ratio (*straight line*) and the water contact angle (*straight line with box*) of PS after 60 s Ar plasma treatment obtained at a jet-nozzle to substrate distance of 5 mm

some distinct differences. While the O/C ratio on PS was at its maximum in the centre of the polymer (position '0') (Fig. 7), the highest O/C ratio on PE was besides the area where the jet directly impinged the surface (Fig. 6). Furthermore, Fig. 7 clearly indicates the correlation between the radial profile of the wettability and the radial distribution of the O/C ratio of PS. The lowest water contact angle was measured where the highest O/C ratio was determined. It is well known that the incorporation of oxygen on the polymeric surface results in the formation of functional groups. Therefore, the changes in carbon bindings were analyzed by fitting the high resolution C 1s peak. Figure 8 shows the highly resolved measured C 1s spectra of non-treated PE (Fig. 8a) and PS (Fig. 8b) compared to the treated ones. The C 1s spectrum of non-treated PE (dashed line) showed the expected C–H/C–C_{aliph} binding at a binding energy (BE) of 285.0 eV whereas the C 1s spectrum of non-treated PS (dashed line) was mainly composed of C–C_{arom} binding at BE of 284.6 eV (carbon atoms in the phenyl ring), C–H/C–C_{aliph} at BE of 285.0 eV (aliphatic carbon), and the characteristic $\pi \rightarrow \pi^*$ shake-up transition at BE of 291.7 eV arising from the electrons of the aromatic ring [35]. Curve-fitting of the highly resolved C 1s peak of PE after 60 s Ar

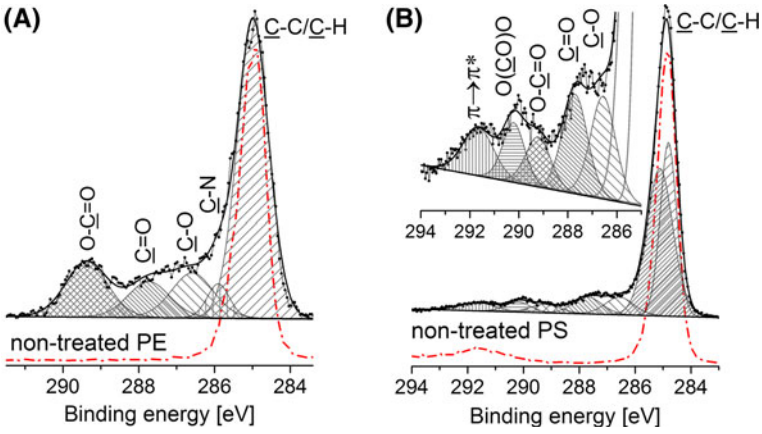

Fig. 8 Highly resolved measured C 1s peak of: **a** non-treated PE (*straight line with dash*) and Ar plasma-treated PE. Also shown is the peak fit of plasma-exposed PE. **b** non-treated PS (*straight line with dash*) and Ar plasma-treated PS. The inset contains the magnification of the peak fit of plasma-treated PS. (Treatment conditions: 5 mm jet-nozzle to substrate distance, 60 s)

Fig. 9 10 × 10 μm AFM images (2-D and 3-D) of PS exposed to Ar (for **b**: 30 s; **c**: 60 s; **d**: 180 s) and Ar + 1 % O_2 (for **e**: 30 s; **f**: 60 s; **g**: 180 s) plasma. The jet-nozzle to substrate distance was 5 mm. Image **a** represents non-treated PS. The AFM images were recorded at position '0' of the polymeric substrate ▶

plasma treatment exhibited five components positioned at binding energies of 285.0, 286.0, 286.6, 287.9, and 289.3 eV assigned to –C–C/–C–H, –C–N, –C–O (hydroxyl, ether), –C=O (ketone, aldehyde), and -O–C=O (carboxylic groups, ester), respectively (Fig. 8a). For PS an additional peak at 290.3 eV can be observed after plasma treatment, which was attributed to –O–(C=O)–O (carbonate) groups. The appearance of –O–(CO)–O bindings represents highly oxidized carbon which is characterized by the maximum concentration of bonded oxygen. The formation of –O–(CO)–O is based on the interaction of oxygen with the aromatic phenyl rings which results in ring breaking. Therefore, the C 1s high resolution spectrum of PS before and after plasma treatment showed a decrease in the intensity of the $\pi \rightarrow \pi^*$ shake-up peak from 6.5 to 2.6 % as well as a decrease in the intensity of the $C–C_{arom}$ binding from 62.4 to 49.5 % after plasma treatment. Besides the functionalization of hydrocarbons by oxidation reactions, the surface ablation process is a further effect of plasma treatment which becomes more and more dominant at longer plasma exposure [36]. It is most likely that etching processes are based on chemically reactive species produced by admixture of oxygen. Thus, a breaking of C–C/C–H bonds is initiated, causing the release of low molecular weight fragments, CO_2, and H_2O [37]. Certainly, the etch process influences the surface texture which in turn depends on the process gas [38, 39]. The change in the surface topography of PS with respect to the type of gas and treatment time (30, 60, and 180 s) is shown by selected representative 10 × 10 μm 2-D and 3-D AFM images in Fig. 9. Figure 9a displays the surface topography of non-treated PS characterized by a lamellar structure due to manufacturing process. After 30 s exposure to Ar (Fig. 9b) and Ar/O_2 (1 % O_2) plasma (Fig. 9e), the topography of PS showed no significant changes, the lamellar structure is still visible, only a few surface grains appeared at the surface which was also observed by Teare et al. [40]. PS samples exposed to Ar and Ar/O_2 plasma for 60 s exhibited initial changes in the surface topography characterized by the appearance of several small nanostructures on their surfaces (Fig. 9c, f). Long-time plasma treatment with exposure times above 180 s led to an increase of the number of grains and the formation of spikes of considerable height. The difference between the surfaces treated with Ar and Ar/O_2 plasma is noticeable: after Ar/O_2 plasma treatment the surface was characterized by a multitude of spikes and grains, the lamellar structure of the non-treated PS was not recognizable anymore. Furthermore, the spikes on the Ar plasma treated PS surface were not as dense packed as on PS after 180 s Ar/O_2 plasma exposure. These dramatic changes in the surface topography can be attributed to the admixture of oxygen leading to the generation of chemically reactive species etching the polymer surface. The results of the determined surface roughness R_{rms} and R_a varied between 2–3 nm for R_a and 2–4 nm for R_{rms}, respectively, independent on whether the PS surface is exposed to plasma or not. Hence, the R_{rms} and R_a values are not indicative of showing differences concerning the topography of non-treated and plasma-treated PS. Nevertheless, some insight can be gained from the information on the particle size extracted from the corresponding histogram of the AFM images depicted in Fig. 10. The histogram of an AFM image is a height distribution function and provides information on the probability that a spot has a defined height on the scanned area. Figure 10 shows, that the distribution of the particles sizes after plasma treatment was different compared to that of the non-treated PS. Whereas the particle size of the structure on the non-treated PS surface (Fig. 10a) varied between 20 and 40 nm a shift was observed to smaller size values after plasma treatment (Fig. 10b–d),

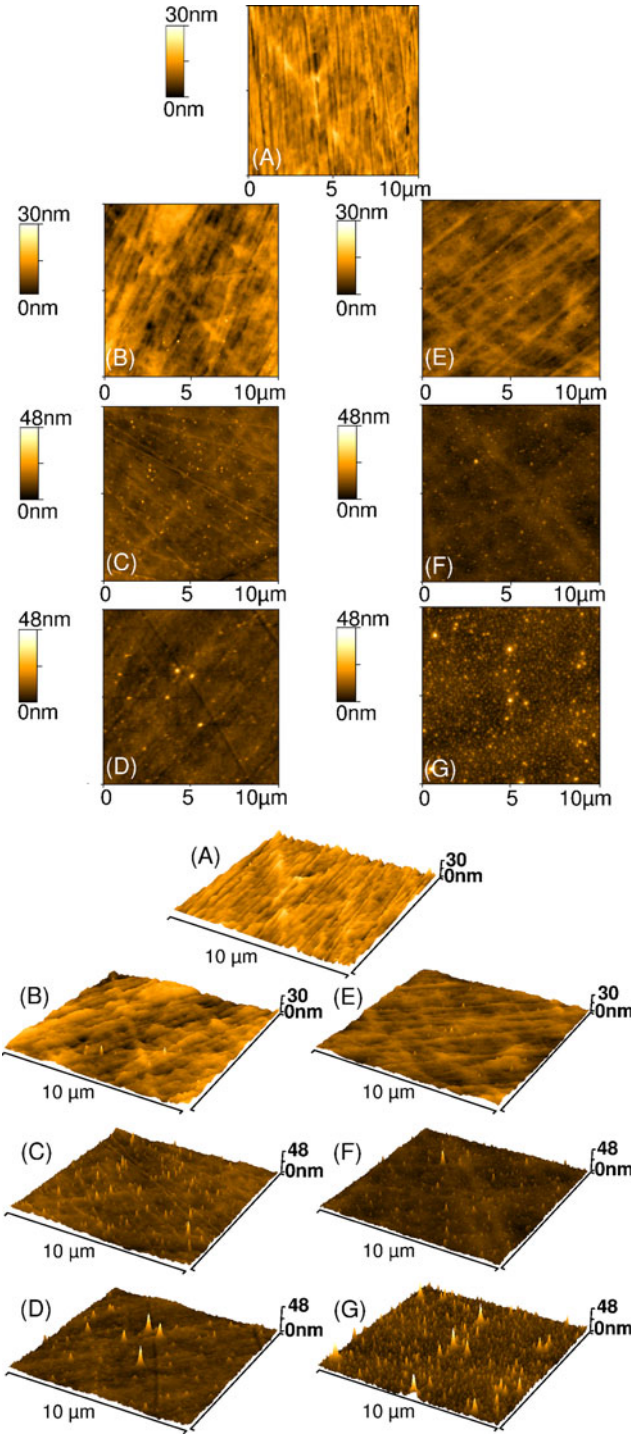
30nm
0nm
(A)
0 5 10μm
30nm
0nm
(B)
0 5 10μm
30nm
0nm
(E)
0 5 10μm
48nm
0nm
(C)
0 5 10μm
48nm
0nm
(F)
0 5 10μm
48nm
0nm
(D)
0 5 10μm
48nm
0nm
(G)
0 5 10μm
(A)
30
0nm
10 μm
(B)
30
0nm
10 μm
(E)
30
0nm
10 μm
(C)
48
0nm
10 μm
(F)
48
0nm
10 μm
(D)
48
0nm
10 μm
(G)
48
0nm
10 μm

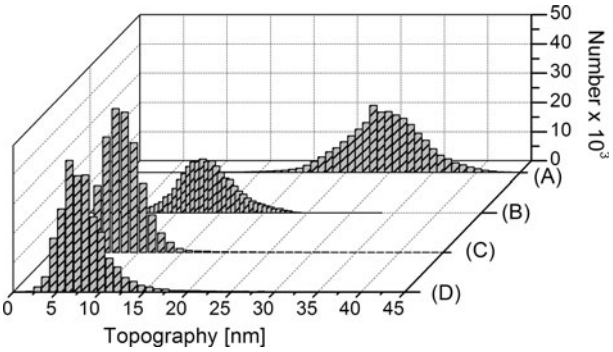

Fig. 10 Histogram derived from the topographic AFM data of: **a** non-treated PS, **b** after 30 s Ar plasma, **c** after 180 s Ar plasma, and **d** after 180 s Ar/O_2 plasma, respectively

most of all after long-time plasma treatment (Fig. 10c, d). Briefly, 180 s Ar/O_2 plasma exposure led to the formation of a uniform surface with spike-like structures and grains showing particle sizes between 5 and 10 nm (Fig. 10d). A similar result was observed for plasma-treated PE. Figure 11 shows a characteristic selection of AFM images of non-treated PE (Fig. 11a) and of PE exposed to Ar plasma (Fig. 11b) and to Ar/O_2 (1 % O_2) plasma (Fig. 11c) for 180 s. The non-treated PE surface was found to be considerably rougher (the R_{rms} value varied between 20 nm and 30 nm) compared to PS and its structure was more granular and hilly. However, a change in the topography of PE was observed after plasma treatment, too. The Ar plasma-treated PE surface was uniformly covered with spikes of similar height whereas Ar/O_2 plasma-treated PE exhibited a surface of densely packed spikes containing many huge spikes. The influence of the jet-nozzle to substrate distance on the morphological changes of the polymers was also investigated. For instance, PS exposed to Ar/O_2 plasma for 180 s at a jet-nozzle to substrate distance of 12 mm showed no morphological differences compared to the non-treated PS (data not shown). After 180 s Ar plasma exposure a few little grains were found on the PS surface. Deduced from these results it can be assumed that etching processes decline with increasing distances to the jet-nozzle which was already reported previously [33].

Conclusions and Outlook

The presented study demonstrated the plasma-based bio-decontamination efficiency of an atmospheric pressure plasma jet operated with argon and different admixtures of molecular oxygen. Plasma inactivation kinetics of *B. atrophaeus* spores indicated that the optimum lethal effect depends on the type of feed gas and the jet-nozzle to substrate distance. Therefore, a maximum reduction of viable number of micro-organisms was achieved after 180 s argon-oxygen (with an admixture of 1% oxygen) plasma operating close to the jet-nozzle. Moreover, it was demonstrated that reactive oxygen species play a determinative role in non-thermal plasma bio-decontamination. Furthermore, this contribution showed to what extent the plasma dose, required for bio-decontamination, influenced the chemical and morphological surface properties of polymers. For the given plasma conditions, all polymers showed a decrease of the contact angle after a few seconds treatment time. Despite the localized plasma treatment in the centre of the substrate, a considerably larger

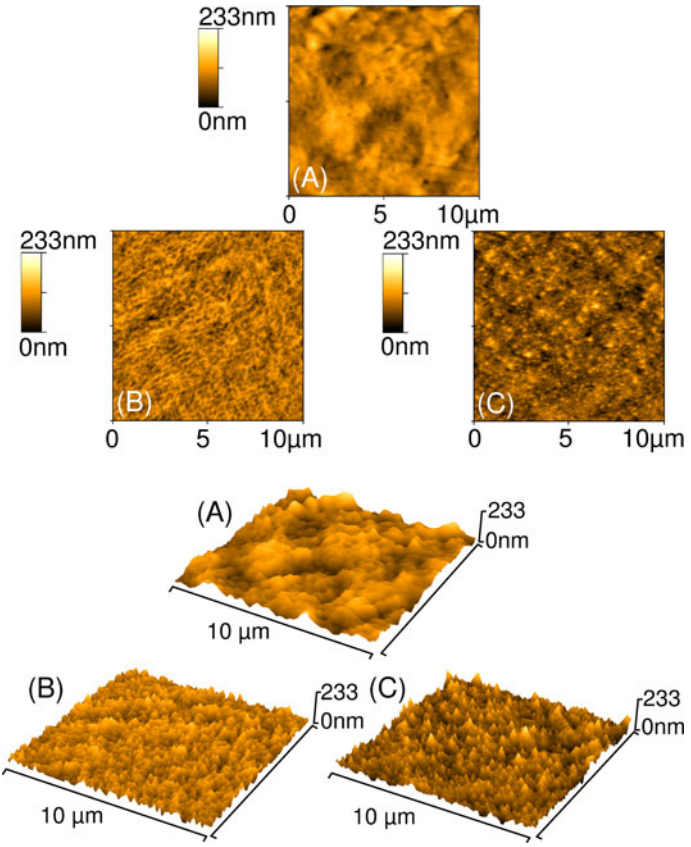

Fig. 11 10 × 10 μm AFM images (2-D and 3-D) of PE. **a** non-treated PE, **b** after 180 s Ar plasma treatment, **c** after 180 s Ar + 1 % O_2 plasma treatment. The jet-nozzle to substrate distance was 5 mm. The AFM images were recorded at position '0' of the polymeric substrate

region was modified far away from the impinging jet. The elemental distribution of PE and PS recorded by X-ray photoelectron spectroscopy showed an incorporation of oxygen due to C–C/C–H bond breaking and the formation of oxygen-containing functional groups, especially C–O, –C=O–, and O=C–O groups. Apart from surface functionalization, also etching processes occurred during the plasma treatment. Etching processes resulted in the formation of a spike-like texture of PE and PS especially when oxygen was added to the argon plasma. Summarizing, short plasma treatment times led to inactivation of micro-organisms and to an effective change in surface properties, for instance of the surface wettability. The plasma assisted improved hydrophilicity and the creation of specific oxygen functionalities on the polymer surface revealed the possibility to enhance the field of applications. Thus, a careful choice of plasma parameters allows for a user-defined tailoring of the surface properties. Since the atmospheric pressure plasma jet can be operated at low temperatures, it offers a promising method of decontamination and modification of heat sensitive material. With regard to cell adhesion, biological response to polymeric materials depends strongly on surface chemistry and structure. Further studies will be performed to investigate the effect of plasma functionalization on cell behavior.

References

1. Chu PK, Chen JY, Wang LP, Huang N (2002) Mater Sci Eng R Rep 36:143
2. van Kooten TG, Spijker HT, Busscher HJ (2004) Biomaterials 25:1735
3. Noeske M, Degenhardt J, Strudthoff S, Lommatzsch U (2004) Int J Adhes Adhes 24:171
4. Moisan M, Barbeau J, Crevier MC, Pelletier J, Philip N, Saoudi B (2002) Pure Appl Chem 74:349
5. Hippler R, Kersten H, Schmidt M, Schoenbach KH (2008) Low temperature plasmas: fundamentals, technologies, and techniques. Wiley VCH vol. 1, Weinheim
6. Laroussi M, Alexeff I, Kang WL (2000) IEEE Trans Plasma Sci 28:184
7. Rupf S, Lehmann A, Hannig M, Schafer B, Schubert A, Feldmann U, Schindler A (2010) J Med Microbiol 59:206
8. Stoffels E, Kieft IE, Sladek REJ, van den Bedem LJM, van der Laan EP, Steinbuch M (2006) Plasma Sources Sci Technol 15:169
9. Weltmann KD, Brandenburg R, von Woedtke T, Ehlbeck J, Foest R, Stieber M, Kindel E (2008) J Phys D Appl Phys 41:6
10. Laroussi M (2005) Plasma Process Polym 2:391
11. Moreau M, Orange N, Feuilloley MGJ (2008) Biotechnol Adv 26:610
12. Ionita ER, Ionita MD, Stancu EC, Teodorescu M, Dinescu G (2009) Appl Surf Sci 255:5448
13. Gomathi N, Mishra D, Maiti TK, Neogi S (2009) J Adhes Sci Technol 23:1861
14. Lommatzsch U, Pasedag D, Baalmann A, Ellinghorst G, Wagner HE (2007) Plasma Process Polym 4:1041
15. Siow KS, Britcher L, Kumar S, Griesser HJ (2006) Plasma Process Polym 3:392
16. Pavithra D, Doble M (2008) Biomed Mater 3:13
17. Gessner C, Bartels V, Betker T, Matucha U, Penache C, Klages CP (2004) Thin Solid Films 459:118
18. Junkar I, Cvelbar U, Lehocky M (2011) Mater Tehnol 45:221
19. Weltmann KD, Kindel E, Brandenburg R, Meyer C, Bussiahn R, Wilke C, von Woedtke T (2009) Contrib Plasma Phys 49:631
20. Lange H, Foest R, Schaefer J, Weltmann KD (2009) IEEE Trans Plasma Sci 37:859
21. Navratil Z, Trunec D, Smid R, Lazar L (2006) Czech J Phys 56:B944
22. Ehlbeck J, Schnabel U, Polak M, Winter J, von Woedtke T, Brandenburg R, von dem Hagen T, Weltmann KD (2011) J Phys D-Appl Phys 44:18
23. Shintani H, Sakudo A, Burke P, McDonnell G (2010) Exp Ther Med 1:731
24. Foest R, Bindemann T, Brandenburg R, Kindel E, Lange H, Stieber M, Weltmann KD (2007) Plasma Process Polym 4:460
25. Laroussi M (2002) IEEE Trans Plasma Sci 30:1409
26. Lim JP, Uhm HS, Li SZ (2007) Phys Plasmas 14:6
27. Schulz-von der Gathen V, Schaper L, Knake N, Reuter S, Niemi K, Gans T, Winter J (2008) J Phys D-Appl Phys 41:6
28. Dobrynin D, Fridman G, Friedman G, Fridman A (2009) New J Phys 11:26
29. Xiong Z, Lu XP, Feng A, Pan Y, Ostrikov K (2010) Phys Plasmas 17:6
30. Bornholdt S, Wolter M, Kersten H (2010) Eur Phys J D 60:653
31. Setlow P (2006) J Appl Microbiol 101:514
32. Brandenburg R, Ehlbeck J, Stieber M, von Woedtke T, Zeymer J, Schluter O, Weltmann KD (2007) Contrib Plasma Phys 47:72
33. Fricke K, Quade A, Ohl A, Schröder K, von Woedtke Th (2009) In: von Keudell A, Winter J, Böke M, Schulz-von der Gathen V (eds) Proceedings of the 19th international symposium on plasma chemistry (ISPC 19), Bochum (Germany) edited by, contr. P1.8.29 (www.ispc-conference.org)
34. Vogelsang A, Ohl A, Steffen H, Foest R, Schröder K, Weltmann KD (2010) Plasma Process Polym 7:16
35. Beamson G, Briggs D (1992) The Scienta ESCA 300 data base. John Wiley & Sons, Chichester
36. Fricke K, Steffen H, von Woedtke T, Schroeder K, Weltmann KD (2011) Plasma Process Polym 8:51
37. Egitto FD (1990) Pure Appl Chem 62:1699
38. Ataeefard M, Moradian S, Mirabedini M, Ebrahimi M, Asiaban S (2008) Plasma Chem Plasma Process 28:377
39. Coen MC, Dietler G, Kasas S, Groning P (1996) Appl Surf Sci 103:27
40. Teare DOH, Ton-That C, Bradley RH (2000) Surf Interface Anal 29:276